December 2005

Porous Biomimetic Microlens Arrays as Multifunctional Optical Structures

Shu Yang
University of Pennsylvania, shuyang@seas.upenn.edu

Joanna Aizenberg
Bell Laboratories

Postprint version. Published in *Materials Today*, Volume 8, Issue 12 Supplement 1, December 2005, pages 40-46.
Publisher URL: http://dx.doi.org/10.1016/S1369-7021(05)71288-8

Porous Biomimetic Microlens Arrays as Multifunctional Optical Structures

Abstract

Microlenses are important optical components that image, detect and couple light. Most synthetic microlenses, however, have fixed position and shape once they are fabricated. Therefore, the attainable range of their tunability and complexity is rather limited. In comparison, biological world provides a multitude of varied, new paradigms for the development of adaptive optical networks. This review discusses a few inspirational examples of biological lenses and their synthetic analogs. We focus on the fabrication and characterization of biomimetic microlens arrays with integrated pores, whose appearance and function are similar to a highly efficient optical element formed by brittlestars. The complex microlens design can be created by three-beam interference lithography. These synthetic microlenses have strong focusing ability, and the structure can be, therefore, used as an adjustable lithographic mask, and a tunable optical device coupled with the microfluidic system. The replacement of rigid microlenses with soft hydrogels provides means for changing the lens geometry and refractive index continuously in response to external stimuli, resulting in intelligent, multifunctional, tunable optics.

Keywords

Microlens arrays with integrated pores

Comments

Postprint version. Published in *Materials Today*, Volume 8, Issue 12 Supplement 1, December 2005, pages 40-46.
Publisher URL: http://dx.doi.org/10.1016/S1369-7021(05)71288-8

Porous Biomimetic Microlens Arrays as Multifunctional Optical Structures

By Shu Yang[1] and Joanna Aizenberg[2]

Abstract

Microlenses are important optical components that image, detect and couple light. Most synthetic microlenses, however, have fixed position and shape once they are fabricated. Therefore, the attainable range of their tunability and complexity is rather limited. In comparison, biological world provides a multitude of varied, new paradigms for the development of adaptive optical networks. This review discusses a few inspirational examples of biological lenses and their synthetic analogs. We focus on the fabrication and characterization of biomimetic microlens arrays with integrated pores, whose appearance and function are similar to a highly efficient optical element formed by brittlestars. The complex microlens design can be created by three-beam interference lithography. These synthetic microlenses have strong focusing ability, and the structure can be, therefore, used as an adjustable lithographic mask, and a tunable optical device coupled with the microfluidic system. The replacement of rigid microlenses with soft hydrogels provides means for changing the lens geometry and refractive index continuously in response to external stimuli, resulting in intelligent, multifunctional, tunable optics.

[1] Department of Materials Science & Engineering, University of Pennsylvania, 3231 Walnut Street, Philadelphia, PA19104, USA. Email: shuyang@seas.upenn.edu.

[2] Bell Laboratories, Lucent Technologies, 600 Mountain Avenue, Murray Hill, NJ 07974, USA. Email: jaizenberg@lucent.com

Overview of biological and biomimetic lens structures

Clear vision is an important adaptation to biological organisms, which in most cases rely on eyes as their photosensory organs for focusing, detection and imaging. Million of years of evolution have perfected the design of the lenses that are used for the image formation by organisms, and resulted in optical structures, whose multifunctional and hybrid characteristics are unparalleled in today's technology.[1] For example, the human eyes have bending lens that dynamically changes focus and gains, and the muscles in the octopus eyes move the lens inward and outward within the shell to focus on close-up and distant objects, respectively. Insects' eyes are made of many mesh-like divisions, which split into many identical imaging units, called ommatidia. Each ommatidium has a corneal lens that can create a field-of-view (FOV) on its own and vary in an angle, which then overlap to provide a composite image of the world to the insect brain. A dragonfly eye contains about 28, 000 ommatidia, which covers a 70^{o} horizontal and 90^{o} vertical range of view. Some vertebrate animals, which need to spend their lives in both air and water, have developed amphibious eyes, allowing them to see clearly in both media. One particular example is seen in the "four-eyed fish" *Analeps*, which uses an ovoid lens with different curvatures on different axes, resulting in two focal lengths and two foveas.

Compared to the multi-faceted roles in bio-optics, the attainable range of tunability and complexity in most technological optical components is rather limited. It will be highly desirable to have complex, robust, and small photonic devices that can mimic the unusual biological designs and functions. Microlens with variable focal length over a wide range is of great interests to increase the efficiency of the light detection, recording,

imaging, and coupling. From simple geometrical optics, the focal length (f) of a thin hemispherical lens can be given by

$$f = R/(n_2 - n_1) \qquad (1)$$

where R is the lens curvature, and n_1 is the refractive index of the surrounding medium, and n_2 is the refractive index of the lens. The focal length of the lens, therefore, is a function of the lens curvature and refractive index contrast. Recently we have developed an electrowetting approach that can dynamically and reversibly change the shape of a liquid microlens by applying some voltage between a conducting liquid and a planar electrode embedded in a dielectric substrate at a certain distance from the liquid - solid interface.[2,3] A different type of tunable fluidic lens is obtained from a thin polydimethylsiloxane (PDMS) membrane sitting on a fluidic chamber bonded to a thin glass slide.[4] Elastic deformation of the membrane occurs when fluid is injected into the lens chamber, mimicking the deformation of lens muscles to change the focal length. A similar approach has been applied to form a convex PDMS lens bonded on a microfluidic chip by varying the pressure in the microfluidic chamber.[5,6] A microdoublet lens consisting of a tunable liquid-filled lens and a solid negative lens, has also been investigated.[7,8] The lens can change shape to bi-convex or meniscus or be filled with different refractive index liquid, which minimizes optical aberrations and maximize the tunability of focal length or field-of-view.

To mimic the complex nervous and visual systems in octopus eyes, a silicon CMOS-based integrated circuit is designed and fabricated to process images based on the brightness, size, orientation and shape.[9] Such electronic vision has potential to be used in robots to see more clearly in dark and murky environments. Artificial ommatidia with

wide FOV are created using microlens-induced self-writing of polymer waveguides.[10] Each ommatidium consists of a self-aligned microlens, a spacer, and a waveguide, resulting in single-peak angular sensitivity with an acceptance angle comparable to their biological counterparts.

In contrast to the above discussed natural optical "eyed" networks, no specialized eyes have been documented in brittlestars, which, however, exhibit a wide range of photic responses. In a light-sensitive brittlestar, *Ophiocoma wendtii,* we have discovered that the single calcite crystals used for skeletal construction are also a component of the photoreceptor, possibly with the function of a compound eye.[11, 12] The periphery of the calcitic skeleton extends into a close-set, nearly hexagonal array of spherical microstructures that display characteristic double-lenslets (Fig. 1). The lenses guide and concentrate light onto photosensitive tissue and offer remarkable focusing ability, angular selectivity and signal enhancement. It is worth noting of an interesting feature of this bio-optical structure, i.e. the presence of a pore network surrounding the lenses, which functions as an adaptive optical device with the "transition sunglasses" capability: the lenses guide and concentrate light onto photosensitive tissue, and the intensity of light reaching the receptors is regulated by the movement of radiation-absorbing intracellular particles through the pores.[12] Thus, the brittlestar microlenses can be considered as an adaptive optical device that exhibits wide-range tunability, including transmission tunability, diaphragm action, numerical aperture tunability, wavelength selectivity, minimization of the "cross-talk" between the lenses, and improved angular selectivity.

Inspired by the unique lens design and the consequent outstanding optical properties in brittlestars, we have been searching for novel approaches to create a

structure that combines microlens arrays with the porous surrounding microfluidic system. Most existing lens fabrication techniques, including inkjet printing[13], melting of patterned photoresists[14], reactive ion etching of silica and silicon[15], soft-lithography[16], or self-assembly of monodispersed polymer beads[17], requires multiple steps to create both lens and pore structures.

Multi-beam interference lithography

Multi-beam interference lithography has been shown as a fast, simple, and versatile approach to create periodic porous microstructures defect free over a large area.[18-20] When two or more optical waves are present simultaneously in the same region of space, the waves interfere and generate periodic variations in intensity and polarization, which can be transferred into a conventional photoresist film (up to 100 μm), to yield periodic lithographic structures with submicron resolution. The photochemistry and lithographic processes involved in multi-beam interference are similar to those in the conventional lithography except that photomasks are not required, and the substrate is transparent since all of the beams are not necessarily launched from the same side of the substrate. Detailed review of multi-beam interference lithography can be found elsewhere.[21]

Interference among any n (≤4) non-coplanar laser beams produces an intensity grating with (n-1) dimensional periodicity, if the difference between their wave vectors is non-coplanar. The intensity distribution of the interference field can be described by a Fourier superposition as the following:

$$I(\mathbf{r}) = \sum_{l=1}^{n}\sum_{m=1}^{n} \boldsymbol{\varepsilon}_l \boldsymbol{\varepsilon}_m^{*} \exp i(\mathbf{k}_l - \mathbf{k}_m)\cdot\mathbf{r} \propto \sum_{l=1}^{n}\sum_{m=1}^{n} a_{lm} \exp i\mathbf{G}_{lm}\cdot\mathbf{r} \quad (2)$$

where, $\boldsymbol{r}$ is the position vector, $\boldsymbol{k}$ and $\boldsymbol{\varepsilon}$ are the wave vector and polarization vector, respectively, a_{lm} is the magnitude. The difference between two of the wave vectors, $G_{lm} = \mathbf{k}_l - \mathbf{k}_m$, where l, m = 1,2, …, n and $l < m$, determines the translational symmetry of the interference pattern.[22-25] The combination of $\Delta\boldsymbol{k}_n$ and $\boldsymbol{\varepsilon}_n$ determines the overall symmetry and contrast of the resulting lattice.[26-29]

Fabrication of porous, biomimetic lens arrays using three-beam interference lithography

The biological lens arrays in brittlestars appear hexagonally packed with surrounding porous structures (see Fig. 1), which suggests that it is possible to synthesize a biomimetic analog using three-beam interference lithography through an appropriate arrangement of beams. We set the three beams to have the same wave vectors, $\boldsymbol{k_1} = 2\pi$ /a $[\,0.035, 0, 0.999\,]$, $\boldsymbol{k_2} = 2\pi$ /a $[\,-0.017, 0.03, 0.999\,]$, $\boldsymbol{k_3} = 2\pi$ /a $[\,-0.017, -0.030, 0.999\,]$, while varying the polarization vectors (see Fig. 2).[30] When the beams are parallel to each other as viewed from $(0, 0, \bar{1})$ direction, the P1 configuration, a periodic variation of light intensity is generated with hexagonal symmetry, and the simulated intensity profile resembles the shape of the biological lens array. In comparison, when the polarization of each wave is perpendicular to the difference between the remaining two wave vectors, the P2 and P3 configurations, a three-fold connectivity with a very small area of highest intensity is observed, suggesting no lens or little lens formation.

By subjecting the interference light to a negative-tone photoresist, SU8, a periodic 2D pattern is obtained corresponding closely to the calculated light intensity distribution (Fig. 2). The highly exposed regions of the photoresists are crosslinked making them

insoluble in an organic developer solution; the unexposed or very weakly exposed regions are dissolved away to reveal holes in the film. In the P1 polarization configuration, when the intensity difference between strongly exposed and adjacent weakly exposed regions is above the threshold, formation of a lens contour is introduced, thus, creating porous hexagonal microlens arrays that are markedly similar to their biological prototype shown in Fig. 1b. The lens contour can be amplified by factors, such as the quantum efficiency of photosensitive molecules (i.e., sensitizers and photoacid generators), the strong nonlinear relationship between the dose, polymerizability and solubility contrast of the photoresists, as well as the shrinkage of resist film during drying. The lens size, shape, symmetry and connectivity are controllable through adjusting the beam wave vectors and their polarizations, while the pore size and porosity are varied by the laser intensity and/or exposure time.

Porous lens arrays as a multipattern photomask

The fabricated microlenses show strong focusing ability. Since the biomimetic design combines two imaging elements – microlens arrays and clear windows – in one structure, it offers unique lithographic capabilities as a "multipattern" photomask.

Photolithographic masks are key components in the fabrication process of patterned substrates. Forming the desired structure on the photoresist layer involves passing light through a mask, which has a pattern of opaque chrome regions that block portions of the wavefront of the light for each exposure.[31] Different patterns generally require different photomasks, whose total cost is high for the multilevel fabrication.[32] Arrays of stacked microlenses can be combined with photomasks in photolithography

process to replicate patterns from photomasks into a photoresist layer[33] or to transfer, for example, macroscopic figures on the mask into multi-level microstructures in the photoresist on a planar substrate in the grayscale reduction lithography process.[16,34] While the latter approach allows controlling the size of the generated features, only one pattern can be generated from each mask. Since microlenses and clear windows would project different light field profiles on a photoresist layer, integration of them in one element in the biomimetic lens arrays offers a new photomask design, allowing direct production of variable microstructures with different sizes in a *single* exposure from a *single* mask. This can be achieved by simply adjusting (i) the illumination dose, (ii) the distance between the mask and the photoresist film, and (iii) the tone of photoresist.[35]

A series of microstructures were patterned on a positive-tone photoresist through the porous microlens arrays, which were separated by a layer of transparent PDMS with variable thickness (see Fig. 3). When the illumination dose is fixed slightly below the sensitivity threshold of the photoresist (I_{th}), no pattern is expected to originate from the light passing through the clear windows, while the focusing activity of the lenses enhances the light field near focus to surpass the resist threshold intensity. For $I < I_{th}$, features in photoresist were selectively generated under the lenses, showing hexagonally packed holes (Fig. 4 a, b). The size of the features in the resist layer, a, can be effectively controlled by placing transparent PDMS spacers with different thickness, h, between the lens and the resist film. For the illumination dose set above the lithographic threshold intensity of photoresist ($I > I_{th}$), patterns originated from both the lenses and the windows were generated (Fig. 4c, d). When $I > I_{th}$ and $h > 2f$, a honeycomb structure was obtained, which was originated from the light coming through the pores only (Fig. 4e).

The microscale honeycomb structures are of interest as 2D photonic crystals with a large bandgap. When $I < I_{th}$, and using a negative tone resist (e.g. SU8), hexagonally packed dots were formed, corresponding to the hexagonal lens array in the mask, while their size was reduced (Fig. 4f).

The "multipattern" lithographic characteristics in the biomimetic lens array was studied quantitatively using simple Fourier optics to simulate the light intensity distribution from both pores and lenses.[36] The pores were assumed to generate a cylindrical light profile, whose peak intensity is determined by the illumination dose, and the lens was assumed to be diffraction limited at its focus. The calculated 3D profiles of the light field generated by the photomask for $I < I_{th}$, $I > I_{th}$, and at different h agree well with the corresponding experimental results shown in Fig. 4.[35]

Integrated microfluidic channels for dynamic tuning of optical properties

As discussed earlier, the integration of microlens and microfluidics offers an attractive possibility to make a tunable optical device. An electrowetting pump in recirculating fluidic channels has been demonstrated to digitally tune the optical fiber properties.[37-39] The electrically controlled and fully reversible motion of the fluid plugs in the channels alters the refractive index profile experienced by the optical waveguide modes of the fiber.

To mimic the migration of pigment-filled chromatophore cells that regulate the light transmission in a porous brittlestar lens array, a simple microfluidic device was assembled to actuate photoactive liquids within the synthetic microlens array (see Fig. 5a-b).[30] When a dye-containing liquid was pumped through the pores, the reduction in

light transmission was detected under optical microscope (Fig. 5c). The percentage of transmission intensity through the lenses can be adjusted depending on the dye concentration and/or thickness of the dye layer covering the lens. By using different liquids (e.g. with selective refractive index and/or including dyes that can absorb a certain wavelength) as surrounding medium between lenses[40], further control over the lens focal length, numerical aperture and wavelength selectivity can be introduced. Potential applications include an optical shutter that turns light on and off in an optical interconnect, and auto-correction of light intensity for spatial vision in bio-imaging.

Synthesis of soft, biomimetic lens arrays from hydrogels

To provide further tunability of optical properties, it will be highly desirable to replace rigid microlenses with soft structures, which could change the geometry and refractive index continuously in response to external stimuli, resulting in intelligent, multifunctional optics. The most obvious choice of the material for such fabrication is hydrogels. As elastic polymers, hydrogels are capable of changing their volume and shape up to several hundred percent in response to pH, temperature, light, electric potential, chemical and biological agents. They have been used in drug delivery and as tissue scaffolds[41, 42], actuators and sensors[43, 44], and recently as temperature sensitive lenses.[45] Most reported hydrogels are, however, prepared from their corresponding liquid monomers by free radical polymerization, which makes them inappropriate for multi-beam interference lithography. The inhomogeneity of the radical formation and the lack of control over the radical diffusion in hydrogels has limited the resolution to 5 μm. Moreover, radical polymerization from liquids is often accompanied with the large volume change during

crosslinking that often causes swelling and collapsing that are detrimental to the formation of complex structured gels. The use of high glass transition temperature (T_g) polymers that can be crosslinked by a better-controlled photoacids-generation mechanism will improve the film mechanical strength, minimize film roughness, and provide better resolution.

Photoacid crosslinkable hydrogel precursors with a high T_g (~100^{o}C), poly(2-hydroxyethyl methacrylate-*co*-methyl methacrylate, PHEMA-*co*-PMMA), were synthesized for the fabrication of soft, biomimetic microlens arrays.[46] We performed three-beam interference lithography of the hydrogel precursors and fabricated soft, highly deformable hydrogel microlens arrays (Figure 6). There was almost no change in the unit size of the microlens arrays in the non-deformed region, in contrast to a large shrinkage typically observed in radical-polymerized hydrogels. A minimum feature size of 600 nm was resolvable.

The use of PHEMA as a hydrogel precusor offers numerous synthetic and functional advantages. It can be copolymerized with various comonomers to realize different 3D hydrogel structures with tailored architectures, tunability and functionalities. For example, using responsive hydrogels as microlens materials, we can dynamically tune the lens shape, size, focal length, and/or refractive index to improve the capabilities of rigid structures. We have recently demonstrated change of focus in response to pH when incorporating 5 mol% poly(acrylic acid) into PHEMA gels.[40] Since the hydrogel precursors are compatible to the sol-gel chemistry, it is possible to prepare highly transparent organic-inorganic nanocomposites[47] to improve mechanical properties of the

hydrogel lens without sacrificing its deformability, as well as to increase the refractive index.

Conclusion

Biological world often provides inspirational examples of multifunctional, hybrid optical systems with advanced properties that have attracted many researchers to mimic their structure and function. The presented fabrication strategies, optical properties, multipattern formation, and tunability of the synthetic microlens arrays with the integrated pores that mimic the sophisticated microlens arrays evolved by brittlestars, demonstrate that the lessons learned from nature may improve our current capabilities to construct new, adaptive, micro-scale hybrid optical devices with multiple functionalities, potentially useful for a wide variety of technological applications.

Acknowledgment

We would like to thank the students, postdocs, and collaborators who were involved in the work described in this review, in particular, Drs. Mischa Megens, Gang Chen and Chaitanya K. Ullal. This work is supported by the National Science Foundation (BES-0438004), and ACS Petroleum Research Fund (# 43336-G7).

References

1. Land, M. F.; Nilsson, D.-E. *Animal Eyes*; Oxford University Press: New York, (2002).
2. Krupenkin, T.; Yang, S.; Mach, P. *Appl. Phys. Lett.* (2003), **82**(3), 316.
3. Yang, S.; Krupenkin, T. N.; Mach, P.; Chandross, E. A. *Adv. Mater.* (2003), **15**(11), 940.
4. Zhang, D.-Y.; Lien, V.; Berdichevsky, Y.; Choi, J.; Lo, Y.-H. *Appl. Phys. Lett.* (2003), **82**(19), 3171.
5. Chen, J.; Wang, W. S.; Fang, J.; Varahramyan, K. *J. Micromech. Microeng.* (2004), **14**(5), 675.
6. Agarwall, M.; Gunasekaran, R. A.; Coane, P.; Varahramyan, K. *J. Micromech. Microeng.* (2004), **14**(12), 1665.
7. Chronis, N.; Liu, G. L.; Jeong, K. H.; Lee, L. P. *Opt. Exp.* (2003), **11**(19), 2370.
8. Jeong, K. H.; Liu, G. L.; Chronis, N.; Lee, L. P. *Opt. Exp.* (2004), **12**(11), 2494.
9. Gopalan, A.; Titus, A. H. *IEEE Trans. Neural Networks* (2003), **14**(5), 1176.
10. Kim, J.; Jeong, K.-H.; Lee, L. P. *Opt. Lett.* (2005), **30**(1), 5.
11. Aizenberg, J.; Tkachenko, A.; Weiner, S.; Addadi, L.; Hendler, G. *Nature* (2001), **412**(6849), 819.
12. Aizenberg, J.; Hendler, G. *J. Mater. Chem.* (2004), **14**(14), 2066.
13. Biehl, S.; Danzebrink, R.; Oliveira, P.; Aegerter, M. A. *J. Sol-Gel Sci.Tech.* (1998), **13**(1-3), 177.
14. Haselbeck, S.; Schreiber, H.; Schwider, J.; Streibl, N. *Opt. Eng.* (1993), **32**(6), 1322.
15. Savander, P. *Opt. Lasers Eng.* (1994), **20**(2), 97.

16. Wu, M. H.; Park, C.; Whitesides, G. M. *Langmuir* (2002), **18**(24), 9312.

17. Lu, Y.; Yin, Y. D.; Xia, Y. N. *Adv. Mater.* (2001), **13**(1), 34.

18. Berger, V.; GauthierLafaye, O.; Costard, E. *J. Appl. Phys.* (1997), **82**(1), 60.

19. Campbell, M.; Sharp, D. N.; Harrison, M. T.; Denning, R. G.; Turberfield, A. J. *Nature* (2000), **404**(6773), 53.

20. Yang, S.; Megens, M.; Aizenberg, J.; Wiltzius, P.; Chaikin, P. M.; Russel, W. B. *Chem. Mater.* (2002), **14**(7), 2831.

21. Moon, J. H.; Yang, S. *J. Macromol. Sci. C: Polym. Rev.* (2005), **45**(4), in press.

22. Yuan, L.; Wang, G. P.; Huang, X. K. *Opt. Lett.* (2003), **28**(19), 1769.

23. Cai, L. Z.; Yang, X. L.; Liu, Q.; Wang, Y. R. *Opt. Comm.* (2003), **224**(4-6), 243.

24. Cai, L. Z.; Yang, X. L.; Wang, Y. R. *J. Opt. Soc. Am. A* (2002), **19**(11), 2238.

25. Cai, L. Z.; Yang, X. L.; Wang, Y. R. *Opt. Lett.* (2002), **27**(11), 900.

26. Su, H. M.; Zhong, Y. C.; Wang, X.; Zheng, X. G.; Xu, J. F.; Wang, H. Z. *Phys. Rev. E* (2003), **67**(5), 056619.

27. Sharp, D. N.; Turberfield, A. J.; Denning, R. G. *Phys. Rev. B* (2003), **68**(20), 205102.

28. Ullal, C. K.; Maldovan, M.; Wohlgemuth, M.; Thomas, E. L. *J. Opt. Soc. Am. A* (2003), **20**(5), 948.

29. Ullal, C. K.; Maldovan, M.; Thomas, E. L.; Chen, G.; Han, Y.-J.; Yang, S. *Appl. Phys. Lett.* (2004), **84**(26), 5434.

30. Yang, S.; Chen, G.; Megens, M.; Ullal, C. K.; Han, Y. J.; Rapaport, R.; Thomas, E. L.; Aizenberg, J. *Adv. Mater.* (2005), **17**(4), 435.

31. Thompson, L. F.; Willson, C. G.; Bowden, M. J. *Introduction to microlithography*; 2nd ed.; American Chemical Society: Washington, DC, (1994).

32. Nonogaki, S.; Ueno, T.; Ito, T. *Microlithography Fundamentals in Semiconductor Devices and Fabrication Technology*; Marcel Dekker: New York, (1998).

33. Völkel, R.; Herzig, H. P.; Nussbaum, P.; Dandliker, R.; Hugle, W. B. *Opt. Eng.* (1996), **35**(11), 3323.

34. Wu, H. K.; Odom, T. W.; Whitesides, G. M. *J. Am. Chem. Soc.* (2002), **124**(25), 7288.

35. Yang, S.; Ullal, C. K.; Thomas, E. L.; Chen, G.; Aizenberg, J. *Appl. Phys. Lett.* (2005), **86**(20), 201121.

36. Hecht, E. *Optics*; 2nd ed.; Addison Wesley: Reading, MA, (1987).

37. Mach, P.; Krupenkin, T.; Yang, S.; Rogers, J. A. *Appl. Phys. Lett.* (2002), **81**(2), 202.

38. Hsieh, J.; Mach, P.; Cattaneo, F.; Yang, S.; Krupenkin, T.; Baldwin, K.; Rogers, J. A. *IEEE Photonics Technol. Lett.* (2003), **15**(1), 81.

39. Cattaneo, F.; Baldwin, K.; Yang, S.; Krupenkin, T.; Ramachandran, S.; Rogers, J. A. *J. Microelectromech. Sys.* (2003), **12**(6), 907.

40. Hong, K.; et al., manuscript in preparation (2005).

41. Hoffman, A. S. *Adv. Drug Del. Rev.* (2002), **54**(1), 3.

42. Bryant, S. J.; Anseth, K. S. *Biomaterials* (2001), **22**(6), 619.

43. Beebe, D. J.; Moore, J. S.; Bauer, J. M.; Yu, Q.; Liu, R. H.; Devadoss, C.; Jo, B. H. *Nature* (2000), **404**(6778), 588.

44. Lee, Y. J.; Braun, P. V. *Adv. Mater.* (2003), **15**(7-8), 563.

45. Serpe, M. J.; Kim, J.; Lyon, L. A. *Adv. Mater.* (2004), **16**(2), 184.

46. Yang, S.; Ford, J.; Ruengruglikit, C.; Huang, Q.; Aizenberg, J. *J. Mater. Chem.* (2005), **15**, 4200.

47. Kameneva, O.; Kuznetsov, A. I.; Smirnova, L. A.; Rozes, L.; Sanchez, C.; Alexandrov, A.; Bityurin, N.; Chhor, K.; Kanaev, A. *J. Mater. Chem.* (2005), **15**(33), 3380–3383.

Captions of Figures:

Fig. 1. Structure of a biological microlens arrays in ophiocomid brittlestars. (**a**) Light-sensitive species *O. wendtii* changes colour markedly from day (left) to night (right). (**b**) Scanning electron micrograph (SEM) of a brittlestar lens design. Scale bar, 50 μm. (**c**) SEM of the cross-section of an individual lens in *O. wendtii*. Reprinted with permission from ref 11. ©2001 Nature. (**d-e**) Schematic presentation of a filtering and diaphragm action of chromatophores. (**d**) Reduced illumination condition (night). (**e**) Highly illuminated condition (day). CP – Pigment-filled chromatophore cell; R – receptor; P – pore; L – lens.

Fig. 2. 2D structures fabricated by 3-beam interference lithography from three different configurations of beam polarizations (shown in double-headed arrows) viewed in the $(0,0,\bar{1})$ direction. Calculated total intensity distributions (middle figures) correspond well to the SEM images (right figures). The brightest region corresponds to the highest intensity of light. An enlarged SEM image is inserted in P2 polarization to better demonstrate a small lens. Scale bar: 5 μm. Reprinted with permission from ref. 30. ©2005 WILEY-VCH Verlag GmbH & Co. KGaA, Weinheim.

Fig. 3. Biomimetic porous microlens array as a multipattern lithographic photomask. (**a**) Schematic presentation of the experiment. (**b**) Illustration of the photomask action at different distances from photoresist, *h*, and different light intensities, *I*. For $I < I_{th}$, only features under the lenses are expected (shown as the bold red lines). Their size, a, will depend on the distance from the focal point, *f*. For $I > I_{th}$, the features under the lenses

will be surrounded by the features originating from the pores (shown as the dotted red lines). For $h > 2f$, only features under the windows are expected. Reprinted with permission from ref. 35. ©2005 American Institute of Physics.

Fig. 4. Examples of photoresist patterns generated using the porous lens arrays as photolithographic masks. (**a**-**e**) from positive tone resists (AZ5209) and f) from a negative tone resist (SU8). (**a**) $I < I_{th}$, $h \sim f$; (**b**) $I < I_{th}$, $h < f$; (**c**) $I > I_{th}$, $h \sim f$; (**d**) $I > I_{th}$, $h < f$; (**e**) $I > I_{th}$, $h > 2f$; (**f**) $I < I_{th}$, $h \sim f$. Reprinted with permission from ref. 35. ©2005 American Institute of Physics.

Fig. 5. Illustration of the transmission tunability through the lens array, using controlled transport of light-absorbing liquid in the channels between the lenses. The microfluidic assembly and actuation is shown in (**a**) and (**b**). Light micrographs were recorded in a transmission mode near the focal point: (**c**) without the light-absorbing liquid, (**d**) with the light-absorbing liquid between the lenses. Reprinted with permission from 30. ©2005 WILEY-VCH Verlag GmbH & Co. KGaA, Weinheim.

Fig. 6. SEM images of hydrogel microlens arrays formed from poly(2-hydroxyethylmethacrylate-*co*-methylmethylmethacrylate). (**a**) In the non-deformed region. (**b**) At the edge of the film where the hydrogel lenses were less crosslinked and not well-connected, the lenses were often found stretched and deformed by the capillary force during drying of the developer, methanol. Reprinted with permission from ref. 46. ©2005 Royal Society of Chemistry.

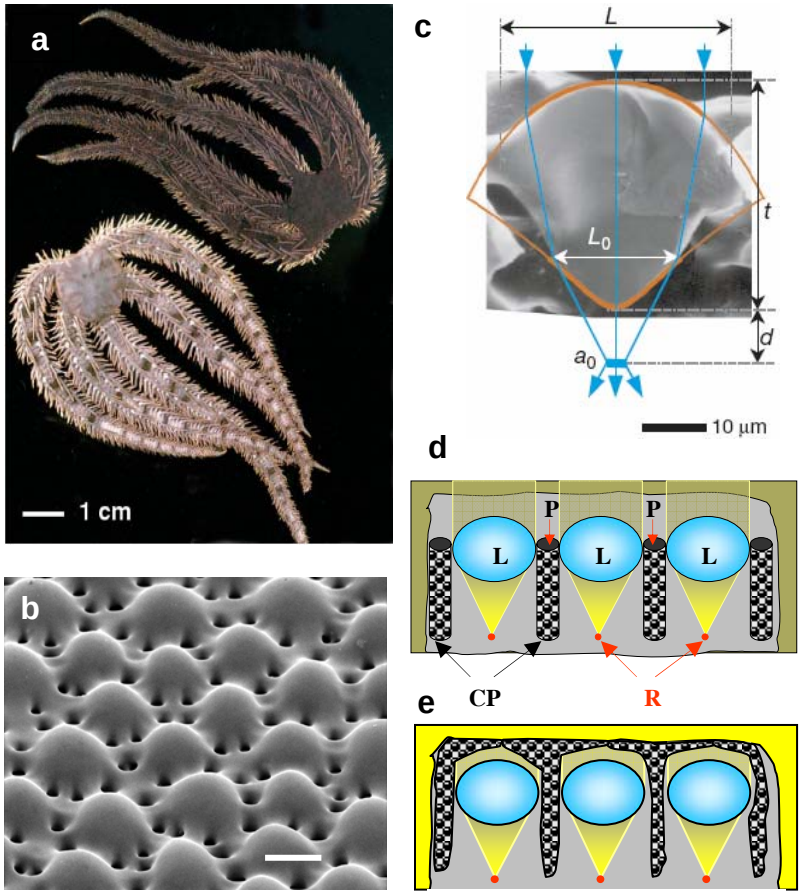

*Fig. 1. Structure of a biological microlens arrays in ophiocomid brittlestars. (**a**) Light-sensitive species O. wendtii changes colour markedly from day (left) to night (right). (**b**) Scanning electron micrograph (SEM) of a brittlestar lens design. Scale bar, 50 µm. (**c**) SEM of the cross-section of an individual lens in O. wendtii. (**b-c**) Reprinted with permission from reference 11. ©2001Nature. (**d-e**) Schematic presentation of a filtering and diaphragm action of chromatophores. (**d**) Reduced illumination condition (night). (**e**) Highly illuminated condition (day). CP – Pigment-filled chromatophore cell; R – receptor; P – pore; L – lens.*

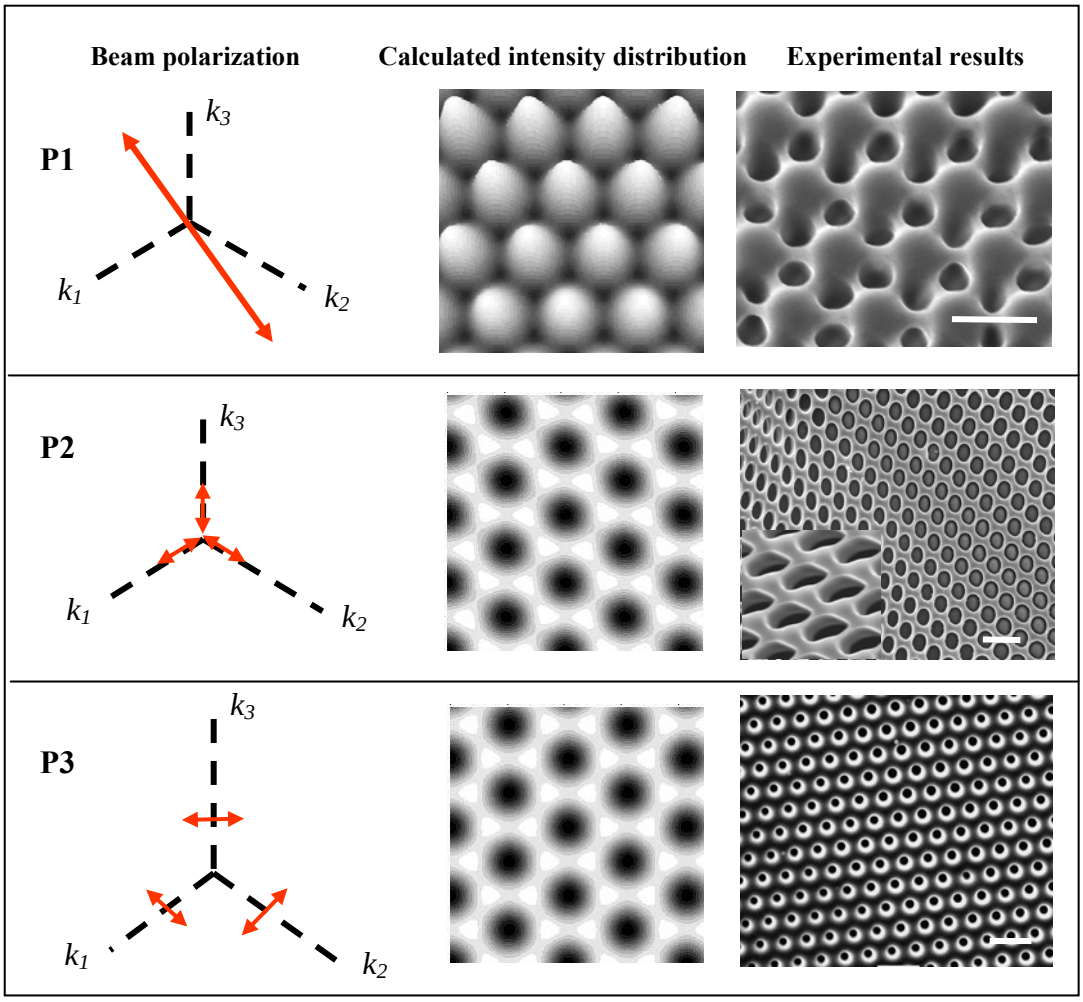

Fig. 2. 2D structures fabricated by 3-beam interference lithography from three different configurations of beam polarizations (shown in double-headed arrows) viewed in the $(0,0,\bar{1})$ *direction. Calculated total intensity distributions (middle figures) correspond well to the SEM images (right figures). The brightest region corresponds to the highest intensity of light. An enlarged SEM image is inserted in P2 polarization to better demonstrate a small lens. Scale bar: 5 μm. Reprinted with permission from ref. 30. ©2005 WILEY-VCH Verlag GmbH & Co. KGaA, Weinheim.*

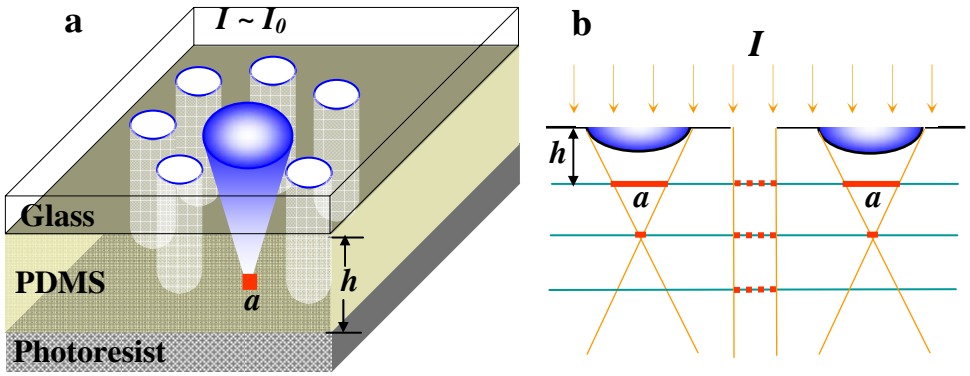

*Fig. 3. Biomimetic porous microlens array as a multipattern lithographic photomask. (**a**) Schematic presentation of the experiment. (**b**) Illustration of the photomask action at different distances from photoresist, h, and different light intensities, I. For $I < I_{th}$, only features under the lenses are expected (shown as the bold red lines). Their size, a, will depend on the distance from the focal point, f. For $I > I_{th}$, the features under the lenses will be surrounded by the features originating from the pores (shown as the dotted red lines). For h > 2f, only features under the windows are expected. Reprinted with permission from ref. 35. ©2005 American Institute of Physics.*

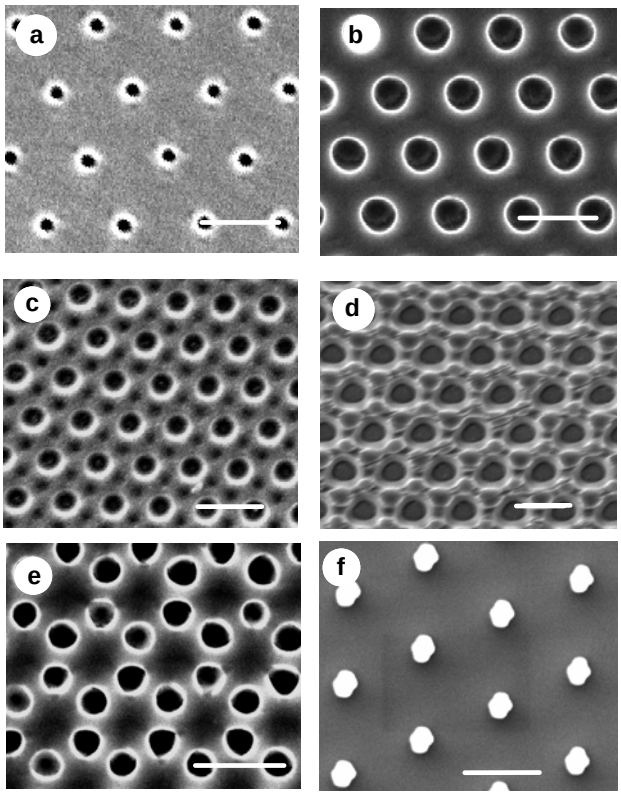

*Fig. 4. Examples of photoresist patterns generated using the porous lens arrays as photolithographic masks. (**a**-**e**) from positive tone resists (AZ5209) and f) from a negative tone resist (SU8). (**a**) $I < I_{th}$, $h \sim f$; (**b**) $I < I_{th}$, $h < f$; (**c**) $I > I_{th}$, $h \sim f$; (**d**) $I > I_{th}$, $h < f$; (**e**) $I > I_{th}$, $h > 2f$; (**f**) $I < I_{th}$, $h \sim f$. Reprinted with permission from ref. 35. ©2005 American Institute of Physics.*

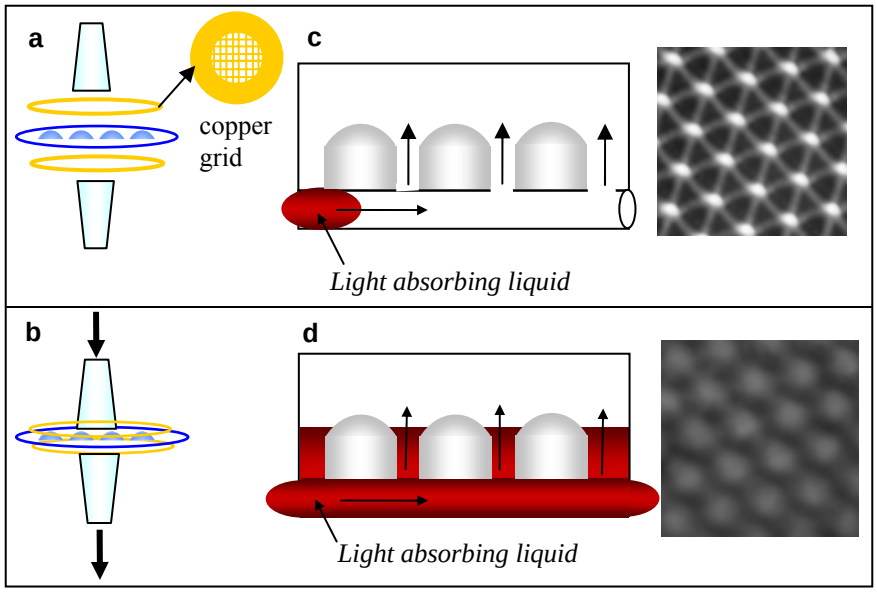

*Fig. 5. Illustration of the transmission tunability through the lens array, using controlled transport of light-absorbing liquid in the channels between the lenses. The microfluidic assembly and actuation is shown in (**a**) and (**b**). Light micrographs were recorded in a transmission mode near the focal point:(**c**) without the light-absorbing liquid, (**d**) with the light-absorbing liquid between the lenses. Reprinted with permission from 30. ©2005 WILEY-VCH Verlag GmbH & Co. KGaA, Weinheim.*

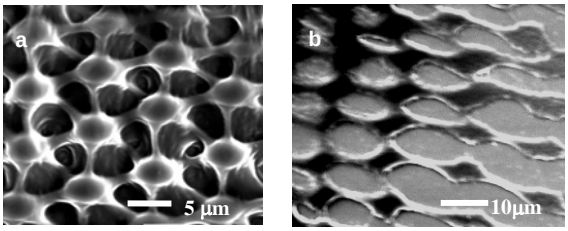

*Fig. 6. SEM images of hydrogel microlens arrays formed from poly(2-hydroxyethylmethacrylate-co-methylmethylmethacrylate). (**a**) In the non-deformed region. (**b**) At the edge of the film where the hydrogel lenses were less crosslinked and not well-connected, the lenses were often found stretched and deformed by the capillary force during drying of the developer, methanol. Reprinted with permission from ref. 46. © 2005 Royal Society of Chemistry.*